PCCP

First principles molecular dynamics simulations of UCln–MgCl2 (n=3, 4) molten salts

Journal:	*Physical Chemistry Chemical Physics*
Manuscript ID	CP-ART-05-2022-002417.R1
Article Type:	Paper
Date Submitted by the Author:	20-Aug-2022
Complete List of Authors:	Li, Bo; University of California, Riverside, Department of Chemistry Dai, Sheng; Oak Ridge National Laboratory, Jiang, De-en; Vanderbilt University

First principles molecular dynamics simulations of UCl_n–$MgCl_2$ (n=3, 4) molten salts

Bo Li,[1] Sheng Dai,[2, 3] and De-en Jiang[4,*]

[1]Department of Chemistry, University of California, Riverside, California 92521, United States

[2]Department of Chemistry, University of Tennessee, Knoxville, Tennessee 37996, United States

[3]Chemical Sciences Division, Oak Ridge National Laboratory, Oak Ridge, Tennessee 37831, United States

[4]Department of Chemical and Biomolecular Engineering, Vanderbilt University, Nashville, Tennessee 37235, United States

*Corresponding author: de-en.jiang@vanderbilt.edu

Abstract

Molten chlorides are a preferred choice for fast-spectrum molten salt reactors. Molten $MgCl_2$ with NaCl forms eutectic mixtures and is considered as a promising dilutant to dissolve fuel salts such as UCl_3 and UCl_4. However, the structure and chemical properties of UCl_n (n = 3, 4) in molten $MgCl_2$ are not well understood. Here we use first-principles molecular dynamics to investigate the molten salt system UCl_n–$MgCl_2$ (n=3, 4) at various concentrations of U^{3+} and U^{4+}. It is found that the coordination environment of Cl^- around U^{3+} especially in the first coordination shell varies only slightly with the uranium concentration and that both the 7-fold coordinate (UCl_7^{4-}) and 6-fold coordinate (UCl_6^{3-}) structures dominate at ~ 40%, leading to an average coordination number of 6.6 – 6.7; network or polymeric structure of U^{3+} cations sharing Cl^- ions is extensively formed when mole fraction of UCl_3 is greater than 0.2. In contrast, the average coordination number of Cl^- around U^{4+} is about 6.4 for mole fraction of UCl_4, x(UCl_4), at 0.1 but decreases to 6.0 for x(UCl_4) = 0.2 and then stays at about 6.0 – 6.2 with the uranium concentration; the 6-fold coordinate structure (UCl_6^{2-}) is the most populous in UCl_4–$MgCl_2$, at about 60%. U-Cl network formation becomes dominant (> 50%) only when x(UCl_4) > 0.5. Unlike Na^+, Mg^{2+} forms network structure with Cl^- ions and when x(UCl_3) or x(UCl_4) < 0.5, over 90% of Mg^{2+} ions are part of a network structure, implying the complex influences from Mg^{2+} on the coordination of Cl around U. The present work reveals the impact of $MgCl_2$ as a solvent for UCl_n (n=3, 4) on the U-Cl coordination and structure as well as motivates further studies of their transport properties and the tertiary systems containing $MgCl_2$-UCl_n.

1. Introduction

Research of molten salt reactors (MSRs) has been reinvigorated recently by the industry, government, and academia, half a century later after they were demonstrated in 1960s.[1-4] In MSRs, the nuclear fuel is dissolved in a molten salt such as UF_4 in LiF-BeF_2-ZrF_4 used in Oak Ridge National Laboratory's molten salt reactor experiment (MSRE). After the fuel salt goes critical in an MSR, the heat is exchanged out by a molten salt coolant for power generation. To facilitate the design and development of the advanced MSRs, it is essential to mapping out the detailed physical and chemical properties of molten salts such as phase diagram, viscosity, heat capacity, and thermal conductivity at the working conditions of MSRs operating at the melting point of the salt.[3, 5] Thorough understanding of the atomic-level interactions, structures, and dynamics of molten salts is beneficial to gather accurate knowledge of these properties and to predict them from first principles.[3-4, 6-11]

Conventional thermal-spectrum MSRs use graphite to slow neutrons down and moderate temperature and employ the fluoride salts such as LiF-BeF_2-ZrF_4 for their high stability, low vapor pressure, and low neutron-capture cross section.[5] New generation of fast-spectrum MSRs use fast neutrons (without the need of a moderator) to sustain the fission chain reaction but requires more enriched fissile material as fuel, thereby necessitating the molten salts for lower viscosity and higher actinide solubility such as chloride-based salts.[2, 12] Compared with thermal-spectrum MSRs, fast-spectrum MSRs can burn the nuclear fuel more completely (thereby reducing the waste) and breed fissile uranium-233 from thorium or fissile plutonium from uranium-238 (thereby having much greater fuel flexibility). For example, the choice of NaCl with another dilutant salt such as $MgCl_2$ is considered a potential candidate to dissolve the fuel salt such as UCl_3.[12] Moreover, molten chlorides have been extensively studied for pyroprocessing of spent nuclear fuel, e.g., the LiCl−KCl eutectic.[13-17] Despite these efforts, there is much less data available for molten chlorides than for molten fluorides relevant to MSRs. And operational molten-chloride MSR has not been experimentally demonstrated yet. Hence there is a great need for both experimental and computational efforts to explore the structure, dynamics, and properties of molten chlorides for fuel salts such as UCl_3 and UCl_4.

NaCl is the top solvent choice for molten-chloride MSR. Previous first principles molecular dynamics (FPMD) simulations have examined the structural change of NaCl−UCl_n (n = 3, 4) melts[18] and previous classical molecular dynamics simulations based on the polarizable-ion model

have studied the relation between the structural and transport properties of NaCl−UCl_3 and predicted an optimal composition based on a heat-transfer figure of merit.[19-20] Machine-learning potentials have been also developed for NaCl-UCl_3 binary systems[8] and fluoride systems[9] based on FPMD simulations. $MgCl_2$ has been proposed as an additional component for the NaCl−UCl_n (n = 3, 4) fuel salt.[12] The liquid structure of $MgCl_2$ is much more complex than that of NaCl, due to the stronger cation-cation correlation.[10, 21-25] To our knowledge, there has been no report on the structural features of UCl_3 and UCl_4 in the $MgCl_2$ molten salt and filling this gap would be conducive to further elucidation of the NaCl-$MgCl_2$-UCl_n (n = 3, 4) tertiary systems for fast-spectrum MSRs. In this work we employ FPMD simulations to investigate the structures of UCl_3 and UCl_4 in $MgCl_2$ molten salt as the concentration varies from 10 mol% to 100 mol%, to shed light on the behavior of the binary $MgCl_2$−UCl_n (n = 3, 4) melts.

2. Computational Details

First principles molecular dynamics (FPMD) simulations were carried out using the Vienna ab initio simulation package (VASP)[26-27] based on density functional theory (DFT) and the Born-Oppenheimer approximation with periodic boundary conditions. The interaction between the electrons and the nucleus was described by the projector augmented wave (PAW) method.[28-29] The Perdew-Burke-Ernzerhof (PBE) functional of the generalized gradient approximation (GGA) was used for electron exchange-correlation.[30] Standard PAW-PBE pseudopotentials were used for Mg ($3s^2$), Cl ($3s^23p^5$), and U ($5f^36d^17s^2$), with a kinetic energy cutoff of 420 eV for the plane wave bases. The Brillouin zone was sampled with the Γ-point only. The dispersion forces were included with the DFT-D3 method.[31] Spin polarization was applied to ensure that U^{3+} and U^{4+} have three and two unpaired electrons, respectively.

Table 1. Details of the simulated UCl_n–$MgCl_2$ (n=3, 4) systems: x, mole fraction; N, formula units; L, lattice parameter of the supercell as a cubic box.

entry	x(UCl_3)	N(UCl_3)	N($MgCl_2$)	L (Å)	entry	x(UCl_4)	N(UCl_4)	N($MgCl_2$)	L (Å)
1	10%	3	27	14.63	8	10%	3	27	14.46
2	20%	6	24	14.74	9	20%	6	24	15.65
3	30%	9	21	14.77	10	30%	9	21	16.04

4	40%	10	15	14.04	11	40%	10	15	15.32
5	50%	12	12	14.07	12	50%	12	12	15.30
6	75%	18	6	14.60	13	75%	15	5	15.57
7	100%	16	0	13.06	14	100%	16	0	14.99

The simulation supercells contain 3 to 18 U atoms and 6 to 27 Mg atoms as well as the corresponding numbers of Cl atoms to model the charge neutral UCl_3−$MgCl_2$ and UCl_4−$MgCl_2$ mixtures. The initial structures of the UCl_n–$MgCl_2$ (n=3, 4) molten salts were generated with Packmol[32] to randomly place the atoms in the simulation box (see the Supporting Information for a comparison between the initial structures and the snapshots after equilibration). We determined the equilibrium volume V_0 of each molten salt mixture by running NVT simulations at different fixed volume V for 10 ps trajectories by setting the temperature to 1200 K. For each simulation, we collected the averaged pressure $P(V)$ from VASP output (calculate as one third of trace of stress-tensor) and fitted it with the corresponding volume V using the Murnaghan equation of state,[33]

$$P(V) = \frac{K_0}{K_0'}\left[\left(\frac{V}{V_0}\right)^{-K_0'} - 1\right],$$

where K_0 is the modulus of incompressibility and K_0' is its first derivative with respect to pressure.

Detailed information for the composition of each supercell is listed in Table 1. The FPMD simulation in the NVT canonical ensemble used a Nosé thermostat[34-35] corresponding to a period of ~40 fs with the time step of 1 fs. We chose the 1 fs time step to make sure that the geometry change in each MD step is sufficiently small to avoid the SCF divergence at the new configuration. The simulation temperature was set at 1200 K, higher than the measured melting points of the UCl_n–$MgCl_2$ (n=3, 4) molten salts and the pure salts (UCl_3, 1146 K; UCl_4, 863 K; $MgCl_2$, 987 K).[36] The total simulation time for each mixture was about 25 ps, in which the first half was considered as equilibration and the second half was used for analysis. With these settings, the energy drifts in our simulations were less than 2 meV/atom-ps.

3. Results and Discussion

3.1. Equilibrium densities

The fitted parameters of the Murnaghan equation of state of UCl_n–$MgCl_2$ (n=3, 4) systems at different uranium concentrations x_U at 1200 K are listed in Table 2 and the fitted pressure-volume curves are shown in Figure 1. From the equilibrium volume V_0, we determined the equilibrium density ρ. As shown in Figure 2, ρ increases linearly with x_U for both and UCl_3−$MgCl_2$ and UCl_4−$MgCl_2$. Our simulated ρ(UCl_4−$MgCl_2$) agrees well with the experimental data:[37] the largest deviation is around 4% when $x_U > 0.7$. Unfortunately, no experimental data are available for UCl_3−$MgCl_2$ to compare with our simulation but for the pure UCl_3 molten salt the good agreement is found between our simulation and experiment.[36] As expected, the density of UCl_3−$MgCl_2$ with its lower U oxidation state is higher than that of UCl_4−$MgCl_2$ at the same x_U and the difference becomes greater with x_U.

Table 2. The fitted parameters of the Murnaghan equation of state for UCl_n–$MgCl_2$ (n=3, 4) systems: x, mole fraction; K_0, the modulus of incompressibility; K_0', the first derivative of K_0, with respect to pressure; V_0, equilibrium volume.

entry	$x(UCl_3)$	K_0 (GPa)	K_0'	V_0(Å^3)	entry	$x(UCl_4)$	K_0 (GPa)	K_0'	V_0(Å^3)
1	10%	2.13	6.52	3132.13	8	10%	2.54	11.52	3025.19
2	20%	2.06	7.41	3201.22	9	20%	1.19	6.62	3813.51
3	30%	2.43	9.47	3221.51	10	30%	1.34	6.60	4129.36
4	40%	2.98	9.03	2765.93	11	40%	1.49	6.57	3596.66
5	50%	2.80	8.04	2777.29	12	50%	1.28	11.27	3583.83
6	75%	2.70	7.00	3110.32	13	75%	0.67	9.06	3775.77
7	100%	2.98	6.89	2227.78	14	100	1.57	5.85	3368.88

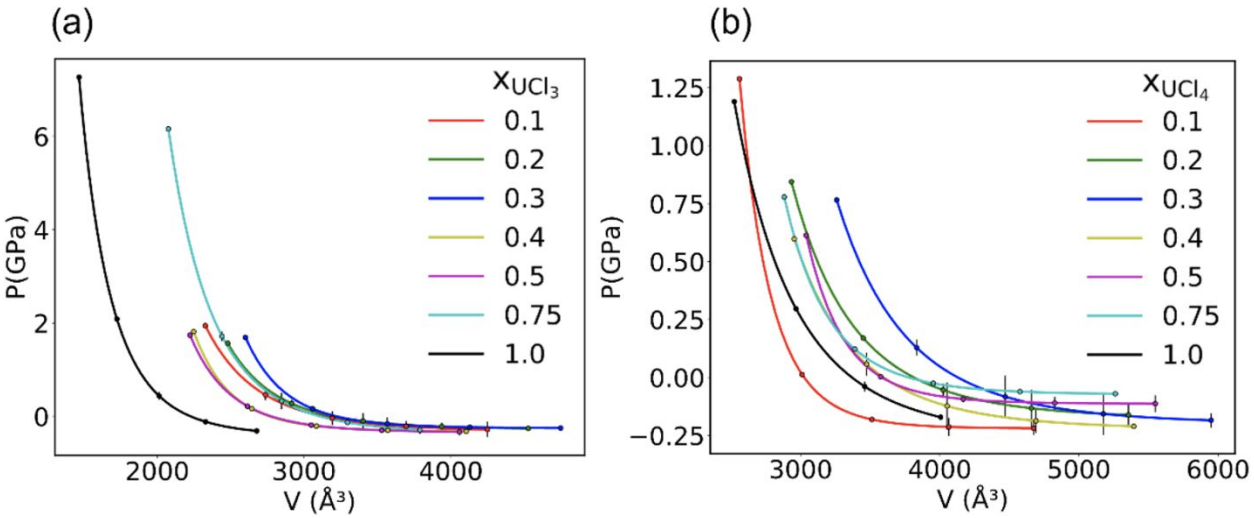

Figure 1. Pressure-volume curves from FPMD simulations at different UCl_n mole fractions using the NVT ensemble: (a) $MgCl_2$-UCl_3; (b) $MgCl_2$-UCl_4. Temperature is set at 1200 K.

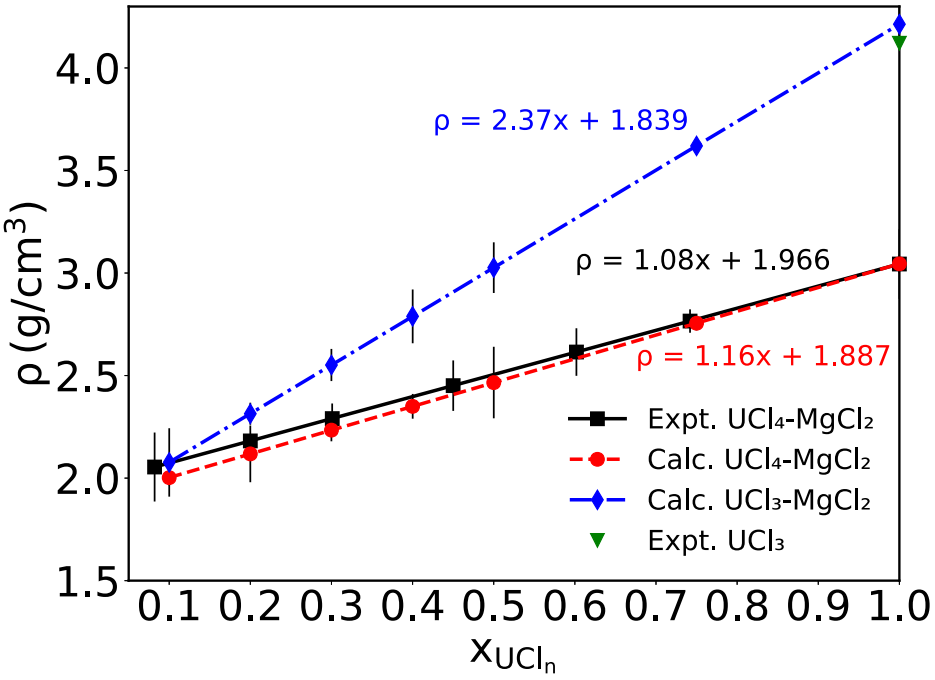

Figure 2. Simulated densities of UCl_3–$MgCl_2$ and UCl_4–$MgCl_2$ molten salts at 1200 K as a function of the mole fraction of UCl_n (x_u) in the melts. Experimental data of pure UCl_3 (green triangle at top right corner) and UCl_4–$MgCl_2$ (black line and squares) are shown for comparison.

3.2. Radial distribution and average coordination number of Cl around U

We then investigated the coordination structure of UCl_3 and UCl_4 in the $MgCl_2$ molten salts at different concentrations. Figure 3 shows the radial distribution function (RDF) and the average coordination number (CN) of U−Cl pair in UCl_3−$MgCl_2$ and UCl_4−$MgCl_2$ molten salts at 1200 K with different mole fractions of UCl_n. The first peak positions in the RDFs at 2.74 Å for UCl_3−$MgCl_2$ (Figure 3a) and 2.63 Å for UCl_4−$MgCl_2$ (Figure 3b) remain constant with UCl_n concentrations, suggesting a stable first coordination shell. Indeed, the average CN of Cl around U in UCl_3−$MgCl_2$ only slightly varies from 6.6 to 6.75 as x(UCl_3) increases from 0.10 to 1.00 (Figure 3c). Likewise, the average CN of Cl around U in UCl_4−$MgCl_2$ varies from 6.0 to 6.2 for x(UCl_4) from 0.20 to 1.00, except at x(UCl_4) = 0.1 where CN=6.4 (Figure 3d). The slightly higher CN of Cl around U^{3+} than around U^{4+} is expected, due to U^{3+}'s greater ionic radius.[38]

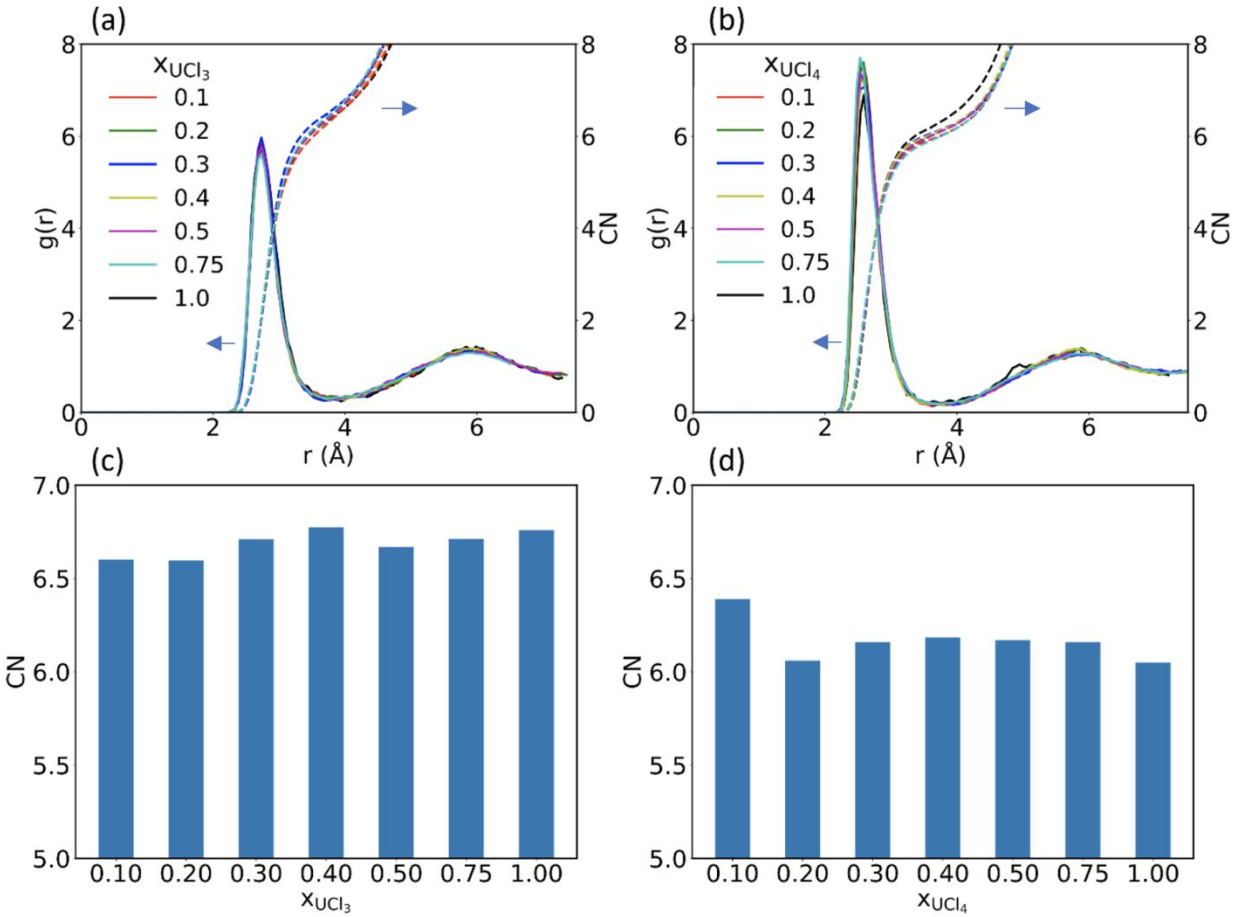

Figure 3. Radial distribution function (solid lines; left axis) and coordination number (CN; dashed lines; right axis) of Cl around U in molten salts of different UCl_n mole factions at 1200 K: (a) UCl_3−$MgCl_2$ and (b) UCl_4−$MgCl_2$. Average CN at different UCl_n mole fractions: (c) UCl_3−$MgCl_2$ (cutoff r = 4.0 Å); (d)

UCl_4–$MgCl_2$ (cutoff r = 3.9 Å). The cutoffs were determined from the average distances at the RDF minima between the first and second coordination shells.

3.3. Radial distribution and average coordination number of Cl around Mg

We next examined the coordination structure of Cl around Mg^{2+} at different UCl_n mole fractions. Figure 4 shows the RDF and the average CN of Mg–Cl pair in UCl_3–$MgCl_2$ and UCl_4–$MgCl_2$ molten salts at 1200 K. The stable first peak at 2.40 Å can be found in both UCl_3–$MgCl_2$ (Figure 4a) and UCl_4–$MgCl_2$ (Figure 4b). The average CN of Cl around Mg in UCl_3-$MgCl_2$ is between 4.5–4.6 (Figure 4c) while larger variance from 4.4 to 4.7 can be seen in UCl_4–$MgCl_2$ (Figure 4d). Of note, our simulated Mg-Cl distance (2.40 Å) and CN of 4.4 for molten $MgCl_2$ are close to the experimental values of 2.42 Å and 4.3, respectively,[23] indicating that the standard PAW potential used here for Mg offers reasonable accuracy. It is also worthwhile in the future to compare with Mg potentials treating core electrons explicitly.

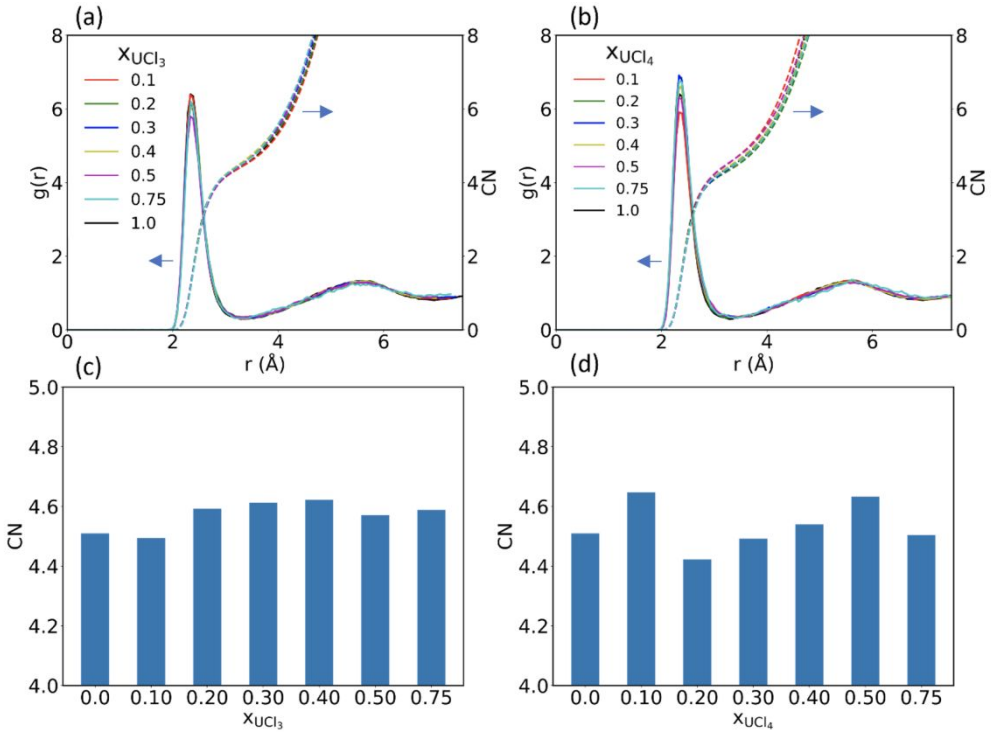

Figure 4. Radial distribution function (solid lines; left axis) and coordination number (CN; dashed lines; right axis) of Cl around Mg in molten salts of different UCl_n mole factions at 1200 K: (a) UCl_3–$MgCl_2$ and (b) UCl_4–$MgCl_2$. Average CN at different UCl_n mole fractions: (c) UCl_3–$MgCl_2$ and (d) UCl_4–$MgCl_2$ with cutoff r = 3.4 Å.

3.4. Change of U coordination environment with concentration

To investigate the diverse coordination environment of a U atom experiencing in a melt, we then decomposed the average coordination number from Figure 3 and analyzed how the distribution of 5-, 6-, 7-, and 8-fold coordination structures of Cl around U change with U concentrations. For UCl_3–$MgCl_2$ (Figure 5a), the 6-fold and 7-fold coordinate structures are the majority, followed by the 8-fold coordinate structure and then the 5-fold coordinate structure. This order is consistent throughout with small variation as x(UCl_3) increases from 0.1 to 1.0. Although the RDFs in Figure 3a suggests a stable first coordination shell, they are an average result, as Figure 5a demonstrates the underlying, relatively constant distribution of different CNs. UCl_4–$MgCl_2$ (Figure 5b) displays a different distribution from UCl_3–$MgCl_2$. The 6-fold coordinate structure dominates in the whole concentration range, fluctuating around 60%. The fraction of the 7-fold coordinate structure drops from 32% to 19% as x(UCl_4) increase from 0.1 to 1.0.

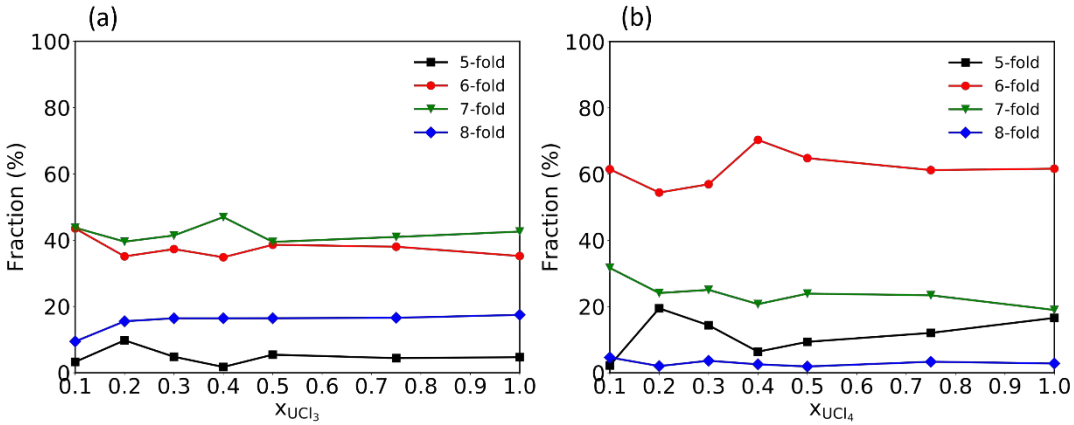

Figure 5. Fractions of 5-fold, 6-fold, 7-fold, and 8-fold coordinates structures of Cl around U in the molten salts of different UCl_n mole fractions: (a) UCl_3–$MgCl_2$ and (b) UCl_4–$MgCl_2$. The coordination structures are defined at an instantaneous snapshot.

3.5. Change of Mg coordination environment with concentration

We then analyzed the coordination environment of Cl^- around Mg^{2+} at the different U concentrations and plotted the fractions of different coordinate structures at different fraction in Figure 6. We can see that in both UCl_3–$MgCl_2$ (Figure 6a) and UCl_4–$MgCl_2$ (Figure 6b) the 4-fold and 5-fold coordinate structures are the majorities with their fractions around 48% and 42%,

followed by about 8% being the 6-fold coordinate structures.

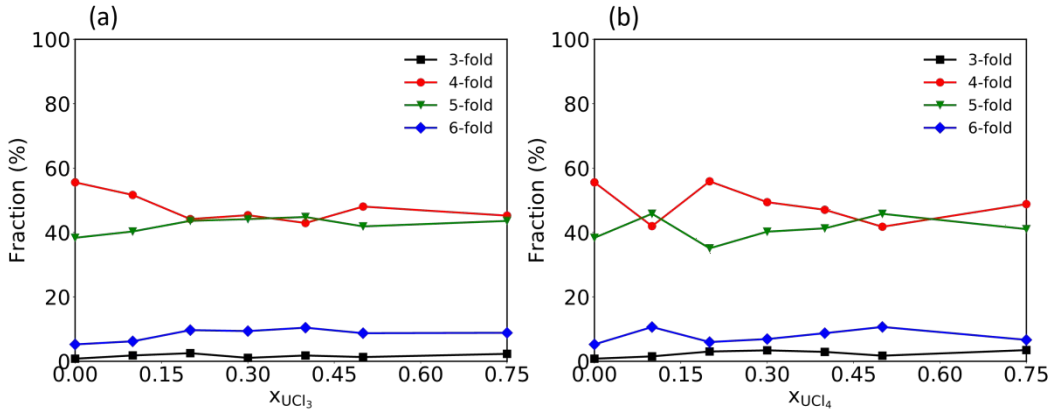

Figure 6. Fractions of 3-fold, 4-fold, 5-fold, and 6-fold coordinates structures of Cl around Mg in the molten salts of different UCl_n mole fractions: (a) UCl_3–$MgCl_2$ and (b) UCl_4–$MgCl_2$. The coordination structures are defined at an instantaneous snapshot.

3.6. Network structure

Network structure formation is common among molten chlorides. The $[UCl_n]^{(n-4)-}$ polyhedra can share corner, edge, or face to form polymers. We analyzed the network formation in UCl_3–$MgCl_2$ and UCl_4–$MgCl_2$. As seen from Figure 7a and Figure 9a, the population of the U–Cl polymers (defined as a network structure containing > 4 U^{3+} cations) in UCl_3–$MgCl_2$ is already close to 50% at the low U concentration and keeps growing as $x(UCl_3)$ increases. At $x(UCl_3)$=0.50, all U ions are in a single cross-linked polymeric network. In contrast, the U–Cl polymers are not found in the UCl_4–$MgCl_2$ until $x(UCl_4)$ > 0.3 (Figure 7b). At low U concentration (< 0.4), the $[UCl_n]^{(n-4)-}$ and $[U_2Cl_n]^{(n-8)-}$ complexes are the main species (Figure 9c) followed by the $[U_3Cl_n]^{(n-12)-}$ and $[U_4Cl_n]^{(n-16)-}$ complexes. As $x(UCl_4)$ increases above 0.40, the U_mCl_n polymer (m > 4) becomes dominant and reaches over 80% only when $x(UCl_4)$ is greater than 0.7.

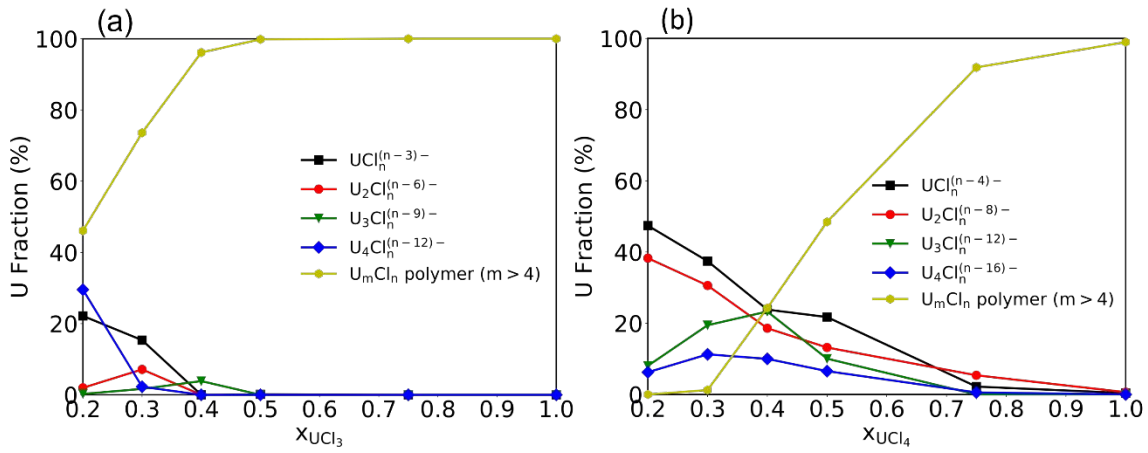

Figure 7. Fractions of U−Cl oligomers at different UCl_n mole fractions in the molten salts: (a) UCl_3−$MgCl_2$ and (b) UCl_4−$MgCl_2$. The oligomer structures are defined at an instantaneous snapshot.

We also analyzed the network structure formed by the Mg−Cl polyhydra (Figure 8). When U concentration is low (< 0.30), Mg concentration is high and all Mg ions are part of a single interconnected network (Figure 9a and Figure 9c). As U concentration further increases, the Mg_mCl_n polymers (m > 4) begin to be broken apart (Figure 9b and Figure 9d). At high U concentration (0.75), the Mg dimers and trimers are more prominent in UCl_4, while the Mg monomer is dominant in UCl_3.

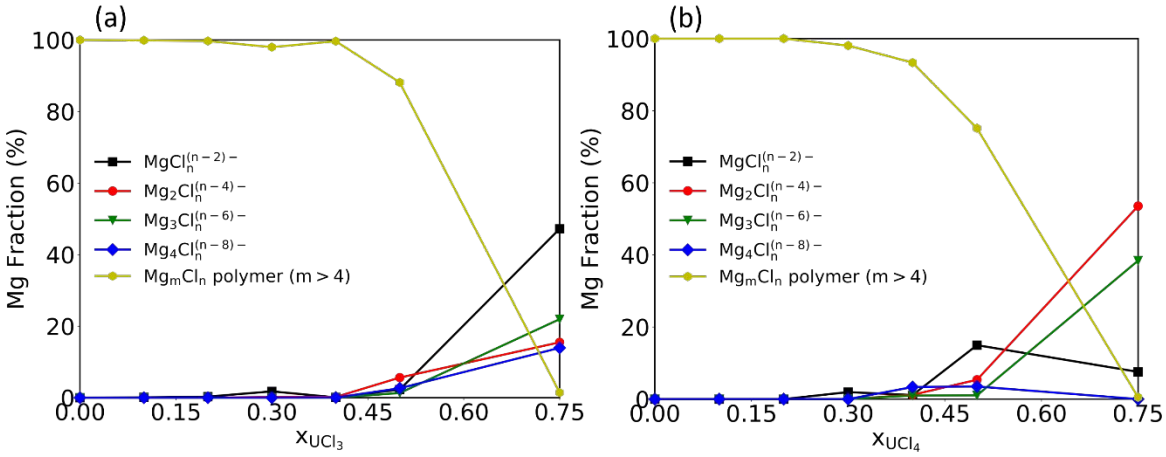

Figure 8. Fractions of Mg−Cl oligomers at different UCl_n mole fractions in the molten salts: (a) UCl_3−$MgCl_2$ and (b) UCl_4−$MgCl_2$. The oligomer structures are defined at an instantaneous snapshot.

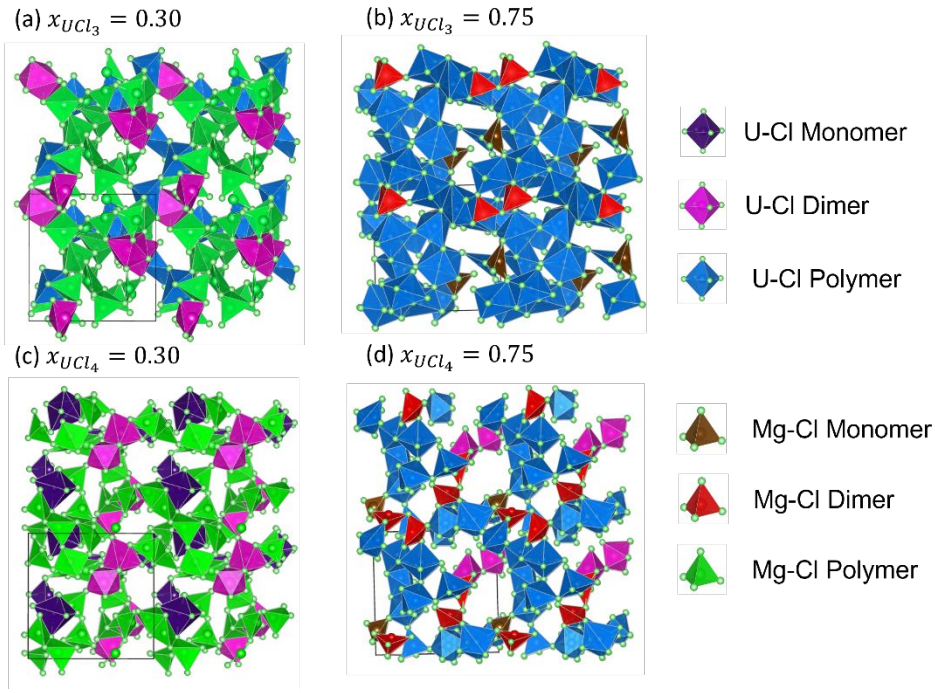

Figure 9. Snapshot of formation of the U−Cl oligomers and Mg−Cl oligomers at different UCl_n mole fractions in the molten salts. Upper: (a-b) UCl_3-$MgCl_2$. Lower: (c-d) UCl_4-$MgCl_2$.

3.7. Comparison of UCl_n–NaCl (n=3, 4) and UCl_n–$MgCl_2$ (n=3, 4)

Comparing to our previous study of UCl_n–NaCl molten salt,[18] we notice that the coordination environment and network involving U^{3+} cations is quite different between UCl_3–NaCl and UCl_3–$MgCl_2$: in the former the coordination number of Cl^- around U^{3+} stays around 6.0 up to $x(UCl_3)$ = 0.5 and the network structure of U^{3+}–Cl^-–U^{3+} is not dominant until $x(UCl_3) > 0.3$; in the latter the coordination number of Cl^- around U^{3+} is higher and remains constant at 6.6 – 6.7 with U concentration and the population of the network structure of U^{3+}–Cl^-–U^{3+} is already close to 50% at $x(UCl_3) = 0.2$. Both differences are closely related to the Mg^{2+}–Cl^-–Mg^{2+} network which makes U^{3+} more concentrated and more Cl^- available to coordinate with U^{3+}. More similarity can be found between UCl_4–NaCl and UCl_4–$MgCl_2$: when $x(UCl_4) > 0.2$, the average coordination number of Cl^- around U^{4+} is about six with the population of the 6-fold coordinate structure dominant in both cases. But the population of the U^{4+}–Cl^-–U^{4+} network structure grows slower in $MgCl_2$ than in NaCl when $x(UCl_4) > 0.3$.

Unlike NaCl molten salt where the single valent Na^+ ions do not form network structures with Cl^- ions,[39] Mg^{2+}–Cl^-–Mg^{2+} chains with intermediate-range order are found in $MgCl_2$ molten salt[21]

and the high tendency of the formation of Mg^{2+}–Cl^{-}–Mg^{2+} network is both found in UCl_3–$MgCl_2$ and UCl_4–$MgCl_2$. With the increasing concentration of UCl_3 or UCl_4, U^{3+}/U^{4+} cations will compete with Mg^{2+} for Cl^{-} ions to form the U^{n+}–Cl^{-}–U^{n+} network structures at the expense of the Mg^{2+}–Cl^{-}–Mg^{2+} oligomers or polymers. One can expect inter-network interactions between Mg^{2+}–Cl^{-}–Mg^{2+} and U^{n+}–Cl^{-}–U^{n+} chains in the intermediate concentration ranges when both are supposed to be present substantially. Given the size and timescale limitations of our FPMD simulations, one hopes to address such issues and their impact on thermophysical and transport properties from the advanced model such as machine learning to accurately describe the change of chemistry due to different oxidation states of U. In addition, it would also be interesting to find out the evolution of such networks in the NaCl-$MgCl_2$-UCl_n. Further study is warranted.

4. Conclusions

We have used first-principles molecular dynamics to investigate the molten salt system UCl_n–$MgCl_2$ (n=3, 4) at various concentrations of U^{3+} and U^{4+}. We found that the coordination environment of Cl^{-} around U^{3+} especially in the first coordination shell remains about the same with the uranium concentration and the 7-fold coordinate and 6-fold coordinate structures dominate both at ~ 40%, leading to an average coordination number of 6.6 – 6.7; network structure formed by U^{3+} cations sharing Cl^{-} ions is extensively formed even at low U concentrations of $x(UCl_3) \sim 0.2$. In contrast, the average coordination number of Cl^{-} around U^{4+} is about 6.4 for $x(UCl_4) = 0.1$ but decreases to 6.0 for $x(UCl_4) = 0.2$ and then stays at about 6.0 – 6.2 with the uranium concentration; the 6-fold coordinate structure is the most populous in UCl_4–$MgCl_2$, at about 60% throughout, followed by the 7-fold coordinate structure varying from ~30% to ~20%. U-Cl network formation in UCl_4–$MgCl_2$ becomes dominant (> 50%) only when $x(UCl_4) > 0.5$. Over 90% of Mg^{2+} ions are part of network structure of Mg_mCl_n polymers ($m > 4$) when $x(UCl_3)$ or $x(UCl_4) < 0.5$, indicating that the Mg-Cl and the U-Cl networks are intertwined especially for UCl_3–$MgCl_2$. The present work therefore reveals the contrast between NaCl and $MgCl_2$ as a solvent for UCl_n–$MgCl_2$ (n=3, 4) and the influence of Mg-Cl network on the U-Cl coordination and structure.

Acknowledgments

This research was supported by the US Department of Energy Office of Nuclear Energy – Nuclear

Energy University Programs (DE-NE0008795).

References

1. Rosenthal, M. W.; Kasten, P. R.; Briggs, R. B., Molten-Salt Reactors: History, Status, and Potential. *Nucl. Appl. Technol.* **1970,** *8*, 107-117.

2. Energy Department News Energy Department Announces New Investments in Advanced Nuclear Power Reactors to Help Meet America's Carbon Emission Reduction Goal. https://www.energy.gov/articles/energy-department-announces-new-investments-advanced-nuclear-power-reactors-help-meet (accessed Jan 29, 2018).

3. Oak Ridge National Laboratory *Report for the US Department of Energy, Office of Nuclear Energy Workshop - Molten Salt Chemistry Workshop*; Oak Ridge National Laboratory: Oak Ridge, TN, April 10 - 12, 2017.

4. Le Brun, C., Molten Salts and Nuclear Energy Production. *J. Nucl. Mater.* **2007,** *360*, 1-5.

5. Grimes, W. R., Molten-Salt Reactor Chemistry. *Nucl. Appl. Technol.* **1970,** *8*, 137-155.

6. Li, Q.-J.; Sprouster, D.; Zheng, G.; Neuefeind, J. C.; Braatz, A. D.; McFarlane, J.; Olds, D.; Lam, S.; Li, J.; Khaykovich, B., Complex Structure of Molten NaCl–CrCl3 Salt: Cr–Cl Octahedral Network and Intermediate-Range Order. *ACS Appl. Energy Mater.* **2021,** *4*, 3044-3056.

7. Roy, S.; Liu, Y.; Topsakal, M.; Dias, E.; Gakhar, R.; Phillips, W. C.; Wishart, J. F.; Leshchev, D.; Halstenberg, P.; Dai, S.; Gill, S. K.; Frenkel, A. I.; Bryantsev, V. S., A Holistic Approach for Elucidating Local Structure, Dynamics, and Speciation in Molten Salts with High Structural Disorder. *J. Am. Chem. Soc.* **2021,** *143*, 15298-15308.

8. Nguyen, M. T.; Rousseau, R.; Paviet, P. D.; Glezakou, V. A., Actinide Molten Salts: A Machine-Learning Potential Molecular Dynamics Study. *ACS Appl. Mater. Interfaces* **2021,** *13*, 53398-53408.

9. Lee, S. C.; Zhai, Y.; Li, Z.; Walter, N. P.; Rose, M.; Heuser, B. J.; Zhang, Y., Comparative Studies of the Structural and Transport Properties of Molten Salt FLiNaK Using the Machine-Learned Neural Network and Reparametrized Classical Forcefields. *J. Phys. Chem. B* **2021,** *125*, 10562-10570.

10. Liang, W.; Wu, J.; Ni, H.; Lu, G.; Yu, J., First-Principles Molecular Dynamics Simulations on the Local Structure and Thermo-Kinetic Properties of Molten Magnesium Chloride. *J. Mol. Liq.* **2020,** *298*, 112063.

11. Agca, C.; McMurray, J. W., Empirical Estimation of Densities in NaCl-KCl-UCl_3 and NaCl-KCl-YCl_3 Molten Salts Using Redlich-Kister Expansion. *Chem. Eng. Sci.* **2022,** *247*, 117086.

12. Holcomb, D. E.; Flanagan, G. F.; Patton, B. W.; Gehin, J. C.; Howard, R. L.; Harrison, T. J. *Fast Spectrum Molten Salt Reactor Options*; ORNL/TM-2011/105; Oak Ridge National Laboratory: Oak Ridge, Tennessee, July, 2011.

13. Zhang, Y.; Song, J.; Li, X.; Yan, L.; Shi, S.; Jiang, T.; Peng, S., First Principles Calculation of Redox Potential for Tetravalent Actinides in Molten LiCl–KCl Eutectic Based on Vertical Substitution and Relaxation. *Electrochim. Acta* **2019,** *293*, 466-475.

14. Song, J.; Shi, S.; Li, X.; Yan, L., First-Principles Molecular Dynamics Modeling of UCl_3 in LiCl-KCl Eutectic. *J. Mol. Liq.* **2017,** *234*, 279-286.

15. Jiang, T.; Wang, N.; Peng, S.; Yan, L., Structural and Transport Characteristics of UCl_3 in Molten LiCl-KCl Mixture: A Molecular Dynamics Simulation Study. *Chem. Res. Chin. Univ.* **2015,** *31*, 281-287.

16. Bengtson, A.; Nam, H. O.; Saha, S.; Sakidja, R.; Morgan, D., First-principles molecular dynamics modeling of the LiCl–KCl molten salt system. *Comput. Mater. Sci* **2014,** *83*, 362-370.

17. Salanne, M.; Simon, C.; Turq, P.; Madden, P. A., Calculation of Activities of Ions in Molten Salts with Potential Application to the Pyroprocessing of Nuclear Waste. *J. Phys. Chem. B* **2008,** *112*, 1177-1183.

18. Li, B.; Dai, S.; Jiang, D.-e., First-Principles Molecular Dynamics Simulations of UCl_n–NaCl (n = 3, 4) Molten Salts. *ACS Appl. Energy Mater.* **2019,** *2*, 2122-2128.

19. Li, B.; Dai, S.; Jiang, D.-e., Molecular dynamics simulations of structural and transport properties of molten NaCl-UCl3 using the polarizable-ion model. *J. Mol. Liq.* **2020,** *299*, 112184.

20. van Oudenaren, G. I. L.; Ocadiz-Flores, J. A.; Smith, A. L., Coupled structural-thermodynamic modelling of the molten salt system NaCl-UCl3. *J. Mol. Liq.* **2021,** *342*, 117470.

21. Wu, F.; Roy, S.; Ivanov, A. S.; Gill, S. K.; Topsakal, M.; Dooryhee, E.; Abeykoon, M.; Kwon, G.; Gallington, L. C.; Halstenberg, P.; Layne, B.; Ishii, Y.; Mahurin, S. M.; Dai, S.;

Bryantsev, V. S.; Margulis, C. J., Elucidating Ionic Correlations Beyond Simple Charge Alternation in Molten $MgCl_2$–KCl Mixtures. *J. Phys. Chem. Lett.* **2019**, 7603-7610.

22. Wilson, M.; Madden, P. A., Short- and Intermediate-Range order in MCl_2 Melts: the Importance of Anionic Polarization. *J. Phys.: Condens. Matter* **1993,** *5*, 6833.

23. Biggin, S.; Gay, M.; Enderby, J. E., The structures of molten magnesium and manganese (II) chlorides. *J. Phys. C: Solid State Phys.* **1984,** *17*, 977.

24. Wu, F.; Sharma, S.; Roy, S.; Halstenberg, P.; Gallington, L. C.; Mahurin, S. M.; Dai, S.; Bryantsev, V. S.; Ivanov, A. S.; Margulis, C. J., Temperature Dependence of Short and Intermediate Range Order in Molten MgCl2 and Its Mixture with KCl. *J. Phys. Chem. B* **2020,** *124*, 2892-2899.

25. Roy, S.; Sharma, S.; Karunaratne, W. V.; Wu, F.; Gakhar, R.; Maltsev, D. S.; Halstenberg, P.; Abeykoon, M.; Gill, S. K.; Zhang, Y.; Mahurin, S. M.; Dai, S.; Bryantsev, V. S.; Margulis, C. J.; Ivanov, A. S., X-ray Scattering Reveals Ion Clustering of Dilute Chromium Species in Molten Chloride Medium. *Chem. Sci.* **2021,** *12*, 8026-8035.

26. Kresse, G.; Furthmüller, J., Efficiency of ab-initio Total Energy Calculations for Metals and Semiconductors using a Plane-wave Basis Set. *Comput. Mater. Sci* **1996,** *6*, 15-50.

27. Kresse, G.; Furthmüller, J., Efficient Iterative Schemes for Ab Initio Total-Energy Calculations Using a Plane-Wave Basis Set. *Phys. Rev. B* **1996,** *54*, 11169-11186.

28. Kresse, G.; Joubert, D., From Ultrasoft Pseudopotentials to the Projector Augmented-Wave Method. *Phys. Rev. B* **1999,** *59*, 1758-1775.

29. Blöchl, P. E., Projector Augmented-wave Method. *Phys. Rev. B* **1994,** *50*, 17953-17979.

30. Perdew, J. P.; Burke, K.; Ernzerhof, M., Generalized Gradient Approximation Made Simple [Phys. Rev. Lett. 77, 3865 (1996)]. *Phys. Rev. Lett.* **1997,** *78*, 1396.

31. Grimme, S.; Antony, J.; Ehrlich, S.; Krieg, H., A Consistent and Accurate Ab Initio Parametrization of Density Functional Dispersion Correction (DFT-D) for the 94 Elements H-Pu. *J. Chem. Phys.* **2010,** *132*, 154104.

32. Martínez, L.; Andrade, R.; Birgin, E. G.; Martínez, J. M., PACKMOL: A Package for Building Initial Configurations for Molecular Dynamics Simulations. *J. Comput. Chem.* **2009,** *30*, 2157-2164.

33. Murnaghan, F. D., The Compressibility of Media under Extreme Pressures. *Proc. Natl. Acad. Sci.* **1944,** *30*, 244-247.

34. Hoover, W. G., Canonical Dynamics: Equilibrium Phase-Space Distributions. *Phys. Rev. A* **1985,** *31*, 1695-1697.

35. Nosé, S., A Unified Formulation of the Constant Temperature Molecular Dynamics Methods. *J. Chem. Phys.* **1984,** *81*, 511-519.

36. Janz, G. J.; Tomkins, R. P. T.; Allen, C. B.; Downey, J. R.; Garner, G. L.; Krebs, U.; Singer, S. K., Molten Salts: Volume 4, part 2, Chlorides and Mixtures—Electrical Conductance, Density, Viscosity, and Surface Tension Data. *J. Phys. Chem. Ref. Data* **1975,** *4*, 871-1178.

37. Katyshev, S. F.; Desyatnik, V. N., Density and surface tension of uranium tetrachloride melts with magnesium and calcium chlorides. *At. Energy* **1981,** *51*, 810-812.

38. Shannon, R., Revised effective ionic radii and systematic studies of interatomic distances in halides and chalcogenides. *Acta Crystallographica Section A* **1976,** *32*, 751-767.

39. Roy, S.; Wu, F.; Wang, H.; Ivanov, A. S.; Sharma, S.; Halstenberg, P.; Gill, S. K.; Milinda Abeykoon, A. M.; Kwon, G.; Topsakal, M.; Layne, B.; Sasaki, K.; Zhang, Y.; Mahurin, S. M.; Dai, S.; Margulis, C. J.; Maginn, E. J.; Bryantsev, V. S., Structure and Dynamics of the Molten Alkali-Chloride Salts from an X-ray, Simulation, and Rate Theory Perspective. *Phys. Chem. Chem. Phys.* **2020**.